# Optoacoustic imaging of the prostate: development toward image-guided biopsy

**Mohammad A. Yaseen**[†]
**Sergey A. Ermilov**
**Hans-Peter Brecht**
**Richard Su**
**André Conjusteau**
Fairway Medical Technologies Inc.
710 North Post Oak Road, Suite 204
Houston, Texas 77024

**Matthew Fronheiser**
Seno Medical Instruments, Inc.
3838 Medical Drive, Suite 101
San Antonio, Texas 78229

**Brent A. Bell**
**Massoud Motamedi**
Center for Biomedical Engineering
University of Texas, Medical Branch
Galveston, Texas 77555

**Alexander A. Oraevsky**[*]
Fairway Medical Technologies Inc.
710 North Post Oak Road, Suite 204
Houston, Texas 77024

**Abstract.** Optoacoustic (OA) tomography has demonstrated utility in identifying blood-rich malignancies in breast tissue. We describe the development and characterization of a laser OA imaging system for the prostate (LOIS-P). The system consists of a fiber-coupled Q-switched laser operating at 757 nm, a commercial 128-channel ultrasonic probe, a digital signal processor, and software that uses the filtered radial back-projection algorithm for image reconstruction. The system is used to reconstruct OA images of a blood-rich lesion induced *in vivo* in a canine prostate. OA images obtained *in vivo* are compared to images acquired using ultrasound, the current gold standard for guiding biopsy of the prostate. Although key structural features such as the urethra could be identified with both imaging techniques, a bloody lesion representing a highly vascularized tumor could only be clearly identified in OA images. The advantages and limitations of both forward and backward illumination modes are also evaluated by collecting OA images of phantoms simulating blood vessels within tissue. System resolution is estimated to be 0.2 mm in the radial direction of the acoustic array. The minimum detectable pressure signal is 1.83 Pa. Our results encourage further development toward a dual-modality OA/ultrasonic system for prostate imaging and image-guided biopsy. © *2010 Society of Photo-Optical Instrumentation Engineers.*
[DOI: 10.1117/1.3333548]

## 1 Introduction

Prostate cancer is the most frequently diagnosed type of cancer in men in the United States, with approximately 200,000 new cases of prostate cancer identified each year. It is estimated that in 2009, 27,360 men in the United States will die from prostate cancer. In the United States, prostate cancer is the leading cause of cancer fatalities among men, and it is the third leading cause worldwide.[1,2]

Several methods exist to screen for prostate cancer. Currently, blood screening for prostate-specific antigen (PSA), digital rectal examination (DRE), and tissue biopsy guided by transrectal ultrasound (TRUS) are the most widely accepted diagnostic methods for prostate cancer in clinics.[3,4] However, these techniques all have limited ability to resolve malignant tissue from benign enlarged prostate tissue.[5,6] Physicians typically overcome their limited sensitivity and specificity by using combinations of these methods to perform more accurate diagnoses.[7,8] Although the entire prostate anatomy can be easily visualized by traditional TRUS imaging, malignant lesions are difficult to identify using TRUS. Frequently, evaluating other image factors such as prostate asymmetry and capsular distortion serve as the only indicator of cancer in TRUS images. Although 60 to 75% of prostate malignancies are hypoechoic, they are known to vary in echogenicity, depending on the tumor stage, size, and location.[8] Particularly, TRUS is not suitable for imaging early stage tumors that provide weak echo contrast from normal tissue. In addition to TRUS, a number of imaging techniques exist that provide spatial information of prostate tissue, including magnetic resonance imaging (MRI) and computed tomography (CT).[7–10] All prostate imaging methods currently lack the necessary contrast and sensitivity to independently perform detailed evaluation and staging of malignant tissue. Instead, these techniques serve primarily either to provide complementary spatial information about prostate dimensions or for guidance during needle biopsy.[10] Improved identification of suspicious regions for needle biopsy could potentially enhance chances for early diagnosis and successful therapy. One approach to facilitate image-guided biopsy of the prostate involves combination of TRUS and near-infrared (NIR) diffuse optical tomography.[11] Initial results proved that prostate tumors can be visualized optically due to substantial absorption contrast of the blood-rich tumors, however, the image resolution was suboptimal.[12] Another technology, which is also based on optical contrast of

[†]Current affiliation: Athinoula A. Martinos Center for Biomedical Imaging, Massachusetts General Hospital, Building 149, 13th Street, Charlestown, MA 02129
[*]Address all correspondence to: Alexander A. Oraevsky, PhD, Fairway Medical Technologies Inc., 710 North Post Oak Road, Suite 204, Houston, TX 77024. Tel: 713-772-7867; Fax: 832-201-9192; E-mail: aoraevsky@fairwaymed.com
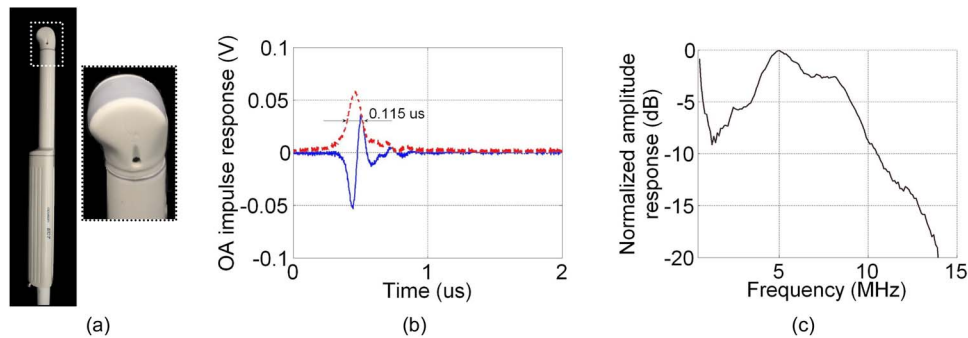
**Fig. 1** (a) Commercial 128-channel endocavity ultrasound probe (EC7ART, Scanhead Corp., San Jose, California) used to collect acoustic transients for OA imaging. The piezoceramic detectors are oriented as a convex array lining the edge of the probe, as seen in the enlarged section. (b) Measured OA impulse response of a single detector in the endocavity probe, where the dashed line indicates envelope-detected signal used for estimation of the radial resolution (see text) and (c) the corresponding frequency response.

the prostate tumors, but could potentially provide better spatial resolution, is optoacoustic imaging.[13,14] In addition to the resolution advantage, optoacoustic imaging can be more conveniently combined with TRUS, because it requires only extra light delivery, and can use the commercial ultrasonic sensor array to receive the generated optoacoustic (OA) signals.

OA images are reconstructed from transient acoustic signals generated by thermal expansion of tissue following the absorption of a short laser pulse.[14] Image resolution orthogonal to the surface of the acoustic probe is determined by the temporal resolution of an individual ultrasonic transducer, and lateral resolution is determined by the angular aperture of the transducer array.[15] The image contrast is provided by the variation in optical absorption within the interrogated tissue. OA cancer imaging takes advantage of the enhanced absorption contrast of blood-rich malignant tissue relative to normal surrounding tissue.[16] To increase beyond 2 to 3 mm in diameter, tumor tissue undergoes angiogenesis, in which a complex network of new microvasculature forms to supply necessary oxygen and nutrients to proliferating tumor cells.[17,18] Prostate carcinomas can, therefore, be distinguished from nonmalignant tissues by elevated density of microvessels.[19] The abnormally high vascular content provides enhanced optical contrast of malignant tumor tissue relative to that of normal tissue in the NIR range, where water and most biomolecules do not substantially absorb light.[20–22]

The utility of OA imaging for detection and characterization of breast tumors has been explored extensively,[16,23–27] and the principles that make OA imaging viable for breast cancer detection offer potential for its utility in detection and characterization of prostate malignancies. Here we report the development of a laser OA system for prostate imaging (LOIS-P). The system utilizes a fiber-coupled NIR laser for maximal optical penetration depth and contrast of blood-rich malignant tissue. Ultrasonic transients are collected using a commercial ultrasound probe containing an array of 128 wide band piezoceramic transducers. Two-dimensional tomographic OA images are constructed from the acquired OA signals using the filtered radial back-projection (RBP) algorithm.[14] As combining OA imaging with ultrasound can provide complementary information regarding the location and vascularity of suspicious lesions,[28] we use both techniques to present images acquired from test phantoms and from *in vivo* canine prostate tissue with mechanically induced blood-filled lesion. Using a three-step computer modeling procedure, we also constructed OA images from simulated *in vivo* conditions to determine the influence of various prostate anatomical features on the OA image.

## 2 Materials and Methods

### 2.1 LOIS-P System Description and Testing

The potential of OA imaging for detecting prostate malignancies was evaluated by imaging surgically exposed canine prostate, illuminated orthogonally, and also blood vessel phantoms imaged in both forward and backward modes. Samples were illuminated with a *Q*-switched alexandrite laser (Ta2, Light Age Inc., Somerset, New Jersey) producing 75-ns laser pulses of 757-nm wavelength at a 10-Hz repetition rate. The laser light was delivered via a bifurcating optical fiber bundle (Dolan-Jenner, Boxborough, Massachusetts) with fluence at the sample surface about 10 mJ/cm². The fiber bundle was comprised of 50-$\mu$m glass fibers, and the terminal bundles measured 4.5 mm in diameter. The laser-generated acoustic transients were collected with a commercial TRUS probe (EC7ART, Scanhead Corp., San Jose, California), pictured in Fig. 1(a). The probe contains an array of 128 piezoceramic transducer elements measure $6 \times 0.2$ mm each with a pitch of 0.21 mm. The transducers line the edge of a convex circular arc segment with a radius of 10 mm and total arc angle of 154 deg, as seen in the enlarged section of Fig. 1(a). The probe also contains an acoustic lens situated directly in front of the transducer array. The lens focuses inside the tissue onto an arc-shaped line with radius of 35 mm located in the imaging plane.

The OA signals acquired from the ultrasonic probe were amplified in two stages and digitized by a 128-channel electronics system. Both analog and digital components were developed by Fairway Medical Technologies (Houston, Texas) for the breast cancer detection system, and were described in a previous publication.[26] Briefly, the first stage consisted of a custom-built charge amplifier with a 30-dB gain for low-noise amplification of capacitive sources. The second amplifier stage was a standard signal amplifier stage with a 30-dB gain. The signals were then digitized by a 12-bit analog-to-digital converter with a maximum sampling rate of 41 MHz.

The impulse response of the probe was collected with a high sampling frequency (1 GHz) using a digital oscilloscope (TDS 3014, Tektronix, Beaverton, Oregon) operated at a high input impedance of 1 M$\Omega$ to simulate the input of the LOIS-P amplifiers. An OA transient with a Dirac $\delta$ function profile was generated by irradiating a layer of highly absorptive India ink.[29] The probe's frequency response was determined by calculating the absolute value of the impulse response's fast Fourier transform in MATLAB (Mathworks, Natick, Massachusetts). For comparison, the frequency response was also determined for the entire LOIS-P system. In the latter case, the impulse response was collected using the commercial probe, LOIS-P electronics, and LOIS-XP software.

The custom-made LOIS-XP software was used to construct OA images from the digitized signal profiles. The program allows for various types of digital signal filtering and provides a real-time display (updating at 10 Hz) of the processed signals from individual transducers. It uses the directivity-weighed filtered RBP algorithm to generate an image from the OA signals.[14,30]

We utilized digital filtering based on the third derivative of the Gaussian wavelet to process the OA signals.[29] In contrast to simple integration of $N$-shaped OA signals, which produce bell-shaped profiles of velocity potential, the wavelet filter produces steep edges at the boundaries of the absorptive object, thereby increasing the sharpness of the OA image.

## 2.2 OA Imaging of Phantoms in Forward and Backward Detection Modes

To evaluate the feasibility of OA imaging for prostate biopsy, we collected OA images of blood vessel phantoms using either forward or backward detection mode,[16] in which laser illumination of tissue occurs on the opposite or the same side as the acoustic pressure detection, respectively. We constructed OA images of a 1-mm tube oriented orthogonally to the imaging plane and located at various distances from the probe. Light was delivered through the terminal ends of the bifurcating fiber bundle described in Sec. 2.1. For forward mode detection, the bundle ends were positioned at stationary locations within the imaging plane roughly 7 cm away from the detector surface. The bundle ends were angled to direct light to a point 25 mm in front of the detector's surface at the detector probe's acoustic focus. In backward mode, the bundle ends were positioned at stationary locations within the imaging plane behind the detector surface and angled to illuminate an object 2.5 cm in front of the detector. The tube was embedded in a homogeneous absorptive and scattering liquid medium ($\mu_a$=0.2 cm$^{-1}$, $\mu_s$=42.1 cm$^{-1}$, $g$=0.75), and contained an aqueous solution of CuSO$_4$ ($\mu_a$=8.73 cm$^{-1}$). OA signals were collected of a single target positioned at different depths, and were subsequently combined for direct visual comparison of the reconstructed OA images. To combine the images, we summed the raw signals collected for each target position and corrected the total for background.

## 2.3 Computer Modeling

Using our three-step modeling procedure,[27] images were constructed by simulating (1) laser irradiation of prostate tissue, (2) the resultant acoustic transients, and (3) the tomographic image construction using the simulated acoustic transients.

We utilized our optical property measurements[31] from freshly harvested prostate tissue of pigs at $\lambda$=757 nm and Monte Carlo light scattering (MCLS) simulation software[32] to compute the distribution of absorbed optical energy. The prostate gland was modeled as a 3.5-cm-diam sphere ($n$=1.4, $\mu_a$=0.417 cm$^{-1}$, $\mu_s$=41.40 cm$^{-1}$, $g$=0.881). Bladder tissue ($n$=1.4, $\mu_a$=0.014 cm$^{-1}$, $\mu_s$=50.79 cm$^{-1}$, $g$=0.872) surrounded the prostate everywhere. The collapsed urethra was depicted as a cylindrical tube passing through the center of the sphere with a 3-mm diameter ($n$=1.4, $\mu_a$=0.240 cm$^{-1}$, $\mu_s$=43.31 cm$^{-1}$, $g$=0.651). A 3-mm-diam sphere represented a highly vascularized malignancy with optical properties identical to those of the prostate, with the exception of $\mu_a$. It was assumed that blood is the primary absorptive tissue component in the NIR range, and that the microvessel density of the lesion was approximately twice that of the surrounding tissue. Therefore, in our Monte Carlo (MC) simulations, $\mu_a$ for the lesion was set to 0.834 cm$^{-1}$. Light illumination was done parallel to the urethra using a 30-mm-diam Gaussian beam.

Using the light absorption volumes from the MC simulations, we modeled the acoustic transient signals received by the detectors.[27] Each cubic voxel from the MC simulation was represented in the acoustic model by the corresponding inscribed sphere. Each sphere, with radius $r_0$, generated an $N$-shaped acoustic transient signal proportional to the absorbed optical energy within the corresponding voxel. The signals were attenuated by acoustic diffraction with $r_0/r$ dependence, where $r$ represents the distance from the center of the sphere to the specified point in space. Each $N$-shaped acoustic signal was convolved with the temporal transducer window.[27] The signals from all spheres were added coherently based on the speed of sound in tissue (1.54 mm/$\mu$s) and their distance from the detector surface. The OA images were constructed from the generated OA signals using the filtered-RBP algorithm described in Sec. 2.1.

## 2.4 In Vivo Imaging of Prostate Tissue

Under a protocol approved by the Institutional Animal Care and Use Committee at the University of Texas Medical Branch (Galveston, Texas), the feasibility of *in vivo* OA imaging of prostate tissue was explored using a live dog. The dog was anesthetized with a mixture of 20 mg/kg Pentothal IV and 0.5 to 2% halothane. To facilitate imaging, the dog's prostate was surgically exposed and placed on the colon. After the initial imaging with LOIS-P, a 17G hypodermic needle was inserted from the superior side of the right lobe (adhering to the conventional prostate geometry utilized in urology). An abrasive brush was inserted through the needle and rotated to create a bloody lesion simulating a cancerous tumor with high blood content. The induced lesion was 3 mm in diameter and located 20 mm deep inside the prostate tissue. OA as well as the control TRUS images were acquired. Finally, the prostate was excised and the animal was humanely sacrificed by intravenous injection of 20 cc of potassium chloride solution, in accordance with recommendations from the Panel on Euthanasia of the American Veterinary Medical Association.

Irradiation of the exposed prostate tissue was performed in orthogonal detection mode, in which the laser illuminates the tissue from a direction perpendicular to the pressure detection. Illumination light was delivered through a fiber optic cable

(a)                                            (b)
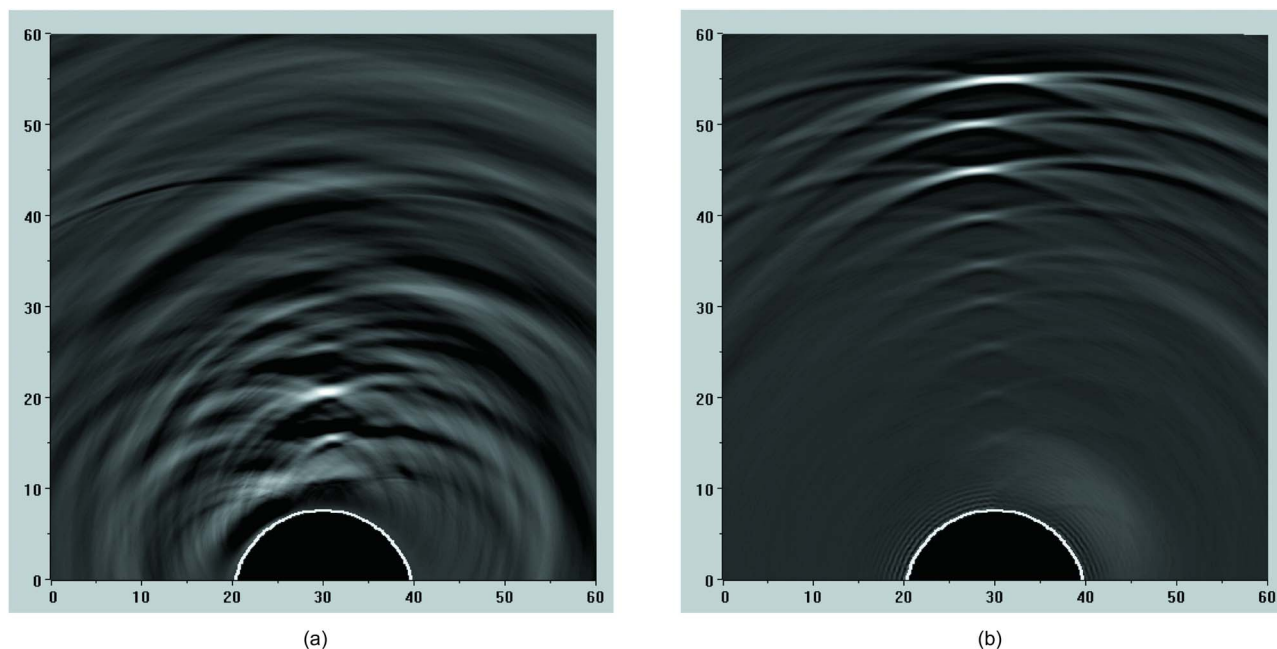
**Fig. 2** Images of combined OA signals for 1-mm cylindrical tube (with the tube axis oriented orthogonal to the imaging plane) positioned at various depths within the aqueous medium simulating optical properties of background tissues, and illuminated using (a) backward OA mode and (b) forward OA mode. OA signals were acquired using a single target, and the images were subsequently created after combining the signals from each individual acquisition. The images are displayed using the standard 8-bit gray-scale palette. The axes are scaled in millimeters.

and a dispersing lens, while the OA probe was pressed firmly against the prostate from the anterior end of the animal. The optical fiber and dispersing lens provided a relatively homogeneous distribution of light within the imaging slice and, therefore, allowed to minimize the image artifacts associated with attenuation of light in the prostate. In this feasibility study, the orthogonal OA mode represented the "best-case scenario" for OA imaging of prostate.

Though TRUS currently lacks the ability to reliably distinguish malignant lesions from benign tissue, it provides detailed spatial information about the prostate. Combining the two imaging techniques has the potential to form high-contrast, high-resolution images, reliably yielding more comprehensive information of the prostate gland and the possible presence of tumors. Therefore, for comparison with OA images and to yield complementary information, ultrasonic images were collected during our *in vivo* imaging experiment using a commercial ultrasound system (3535, BK Medical, Herlev, Denmark) with a 30-mm, 7.5-MHz curved array probe. The system acquired ultrasound images at a rate of 84 frames/s.

## 3 Results

### 3.1 System Characteristics

Figures 1(b) and 1(c) display the detected impulse response and corresponding frequency response, respectively. The frequency response, determined by the fast Fourier transform of the impulse response, shows the probe sensitivity within a 3- to 9-MHz bandwidth ($-6$ dB criterion). The frequency response also shows an undesirable sensitivity band present in the low-frequency range ($<1$ MHz), known to contain large-magnitude acoustic artifacts.[29] Because the LOIS-P amplifier

was designed to operate in wideband mode, the frequency response of the entire LOIS-P system was found to be similar to that of the probe alone (data not shown).

Using the Rayleigh criterion, the minimal distance resolvable in the radial direction of the probe (orthogonal to the array of transducers) was estimated as $a^r_{min} = c_s \tau_{0.5} \approx 0.2$ mm, where $c_s$ denotes the speed of sound in tissue (1.54 mm/$\mu$s), and $\tau_{0.5}$ is the width of the impulse response, transformed to a monopolar waveform using the envelope detection, at the half-max amplitude level (measured to be 115 ns). The maximum sensitivity of the system was measured using a calibrated[29] acoustic emitter (NP/OA90-3, Dapco Industries, Ridgefield, Connecticut) at 5 MHz to be $S = 2.1$ mV/Pa. We assume that the minimum pressure that can be detected with our system occurs when the signal-to-noise ratio (SNR) is 1. Noise data were evaluated for the frequency range between 30 kHz and 10 MHz by collecting and processing recordings with the LOIS-P system in the absence of laser irradiation. The measured root mean squared (rms) noise was $U_{rms} = 3.84 \pm 0.42$ mV. Further analysis revealed that the noise was comprised primarily of white thermoelectric noise, with calculated spectral density of $0.558 \pm 0.093$ $\mu$V/Hz$^{1/2}$. The minimum detectable pressure signal for the system can therefore be estimated as $p_{min} = U_{rms}/S = 1.83$ Pa.

### 3.2 Phantoms Imaged in Forward and Backward Detection Modes

Figure 2 shows OA images of a 1-mm blood vessel phantom located at various distances from the probe. As seen in Fig. 2(a), when the tube is positioned close to the probe ($<15$ mm), the cross section of the tube can be easily seen as a small 1-mm circular source when using the backward OA
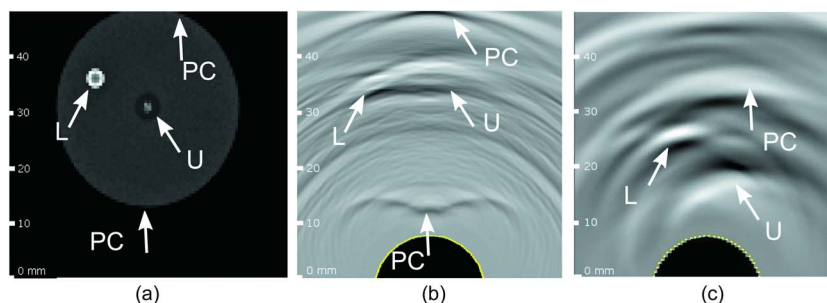
**Fig. 3** Comparison of the modeled OA image with the image acquired *in vivo*: (a) imaging slice showing the distribution of the absorbed optical energy in a prostate model with spherical malignant lesion, determined by MC simulation; (b) OA image constructed using the simulated acoustic transients and the RBP algorithm; and (c) OA image of the dog prostate obtained *in vivo* after inducing a blood-rich lesion. The prostate capsule can be delineated in the OA images. The urethra and the lesion can be seen in the OA images as a dark and bright spots, respectively. The absorption difference between the lesion and surrounding tissue results in high contrast of the OA image. The low absorption in the urethra yields low OA signals. On each image, arrows indicate the prostate capsule (PC), urethra (U), and lesion (L). The images are displayed using the standard 8-bit gray-scale palette.

mode. The deeper vessels in the image cannot be visualized at all. Also, in backward mode imaging, large low-frequency artifacts arise in the OA profiles from nonspecific light absorption in the subsurface volume of tissue and light that reflects back from the illuminated tissue and strikes the detector.[27] These artifacts were reduced in our further studies by proper signal processing and shielding the transducer surface with an optically opaque and acoustically thin polymer layer. In backward OA mode, the magnitudes of the detected OA signals decrease at farther distances from the probe, due to both the attenuation of light as it penetrates within the medium and acoustic diffraction. This combined attenuation effect limits the ability to visualize targets at far distances from the probe with backward mode imaging, as seen in Fig. 2(a).

In forward mode, targets located farther from the probe and closer to the light source produce larger OA signals, as seen in Fig. 2(b). These signals are received by more elements of the detector array, resulting in better contrast in the constructed image. The targets located closer to the probe appear less bright with forward mode imaging also due to attenuation of excitation light. The images are shown in their unprocessed appearance with arc-shaped artifacts caused by the limited aperture of the array of ultrasound transducers. Our group has developed an iterative algorithm based on maximum angular amplitude probability for removal of arc-shaped artifacts and improve contrast and resolution of optoacoustic images.[33] Figure 2, however, is intended to demonstrate gradual loss of lateral resolution with increasing distance from the ultrasonic probe shaped as a convex arc. The dynamic range of the OA image in forward mode is greater than that in backward mode, and was sufficient to visualize all the tubes [Fig. 2(b)].

### 3.3 *Computer-Modeled Images*

We simulated the OA image of malignant prostate tissue under conditions similar to our *in vivo* experiment. Figure 3(a) shows the imaging slice of the absorbed optical energy in the case of the orthogonal OA mode. The lesion is clearly seen as a bright circle implying that it represents a strong OA source. On the other hand, the cross section of the collapsed urethra looks dark, indicating that it is a weak OA source compared to the surrounding prostate tissue. This is further verified by the

reconstructed OA image [Fig. 3(b)], which has major features of the model (the edges of illuminated part of the prostate, urethra, and blood-containing lesion) visible. The OA image constructed from the simulated acoustic transients [Fig. 3(b)] strongly resembles the one constructed from *in vivo* canine prostate [Fig. 3(c)]. The distances of the urethra and lesion from the surface are different between the modeled and experimental images. Furthermore, the portion of the prostate capsule proximal to the probe can be distinguished only in the modeled image. Once more, these differences most likely arise from the fact that tissue compression, which deforms the tissue, is required in the experimental case to achieve acoustic contact.

### 3.4 *In Vivo Images of Prostate Tissue*

Figure 4(a) displays a photograph of the surgically excised prostate sliced through the imaging plane containing the induced lesion, representative of a malignant mass. Upon surgical exposure and without compression, the prostate measured approximately 35 mm along the dorsoventral axis and 50 mm along the dextrosinistral axis. Figure 4(b) shows an image acquired with a commercial ultrasound system. The urethra and the needle insertion path appear in the image as dark, hypoechoic regions. The prostate capsule can also be seen. However, the blood-containing lesion itself does not stand out on the image. Figures 4(c) and 4(d) display OA images of the prostate before and after the lesion was made. In both OA images, the prostate capsule and the urethra can be delineated. The different distances of those objects from the surface of the ultrasonic probe are likely due to slightly higher compression used to achieve acoustic contact in the case of the induced lesion [Fig. 4(d)]. The blood-filled lesion can be resolved in Fig. 4(d) as the bright white area that is absent from Fig. 4(c). The needle insertion path is not visible in both OA images.

## 4 Discussion

Although OA imaging has much potential for diagnosis and treatment monitoring of prostate cancer, a number of factors currently limit its utility. In particular, the delivery of light to prostate tissue presents a challenge for OA imaging. For can-
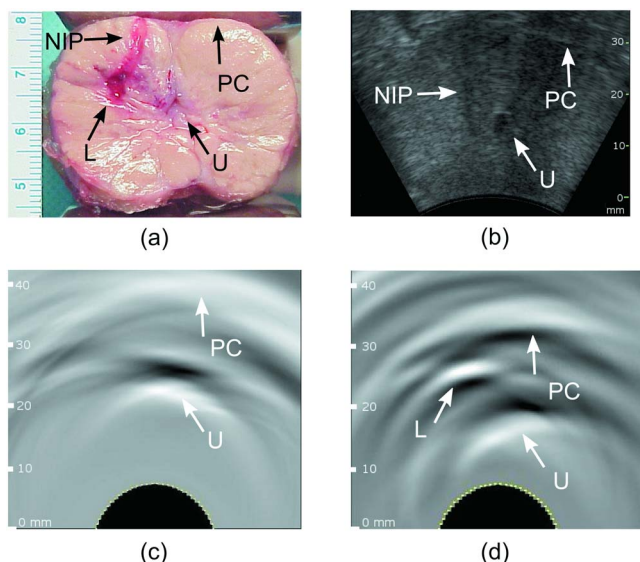
**Fig. 4** (a) Photograph of the sliced dog prostate showing the presence of the induced lesion with blood in the right lateral lobe, the urethra is visible but contracted after surgical excision; (b) ultrasonic image of the same dog prostate obtained *in vivo* after the surgery. OA images of the same dog prostate obtained *in vivo* (c) before and (d) after the lesion was induced. The induced bloody lesion can be seen in (a) and (d). The needle insertion path is visible in (a) and (b). Due to the acoustic mismatch between tissue and air, the prostate capsule can be identified in OA images as a white band. Arrows indicate the prostate capsule (PC), urethra (U), needle insertion path (NIP), and lesion (L). The images are displayed using the standard 8-bit gray-scale palette.

cer detection in a clinic, a minimally invasive strategy is always preferred to ensure patient compliance and minimize discomfort. Therefore, it was initially envisioned that the optimal strategy for OA prostate imaging would require the use of a transrectal probe that both delivers NIR laser light and detects the OA transients of the prostate in backward mode. As mentioned previously, such a probe could be designed by attaching optical fibers to a commercial TRUS probe to illuminate the region directly in front of the ultrasonic (US) detector elements. As the high absorption of the rectal wall can lead to poor prostate illumination and OA image artifacts, we also envisioned an alternative forward detection mode scheme, in which laser illumination and pressure wave detection occur on different sides of the imaged tissue. To achieve this, illumination light can be delivered via a side-firing optical fiber guided through the urethra.

Our phantom studies revealed that forward-mode illumination enabled visualization of all the targets with significant contrast. Unlike the backward OA mode, light is attenuated in the direction toward the probe in the forward OA mode, while acoustic diffraction still increases away from the probe. The two effects partially compensate each other, equalizing the magnitudes of the OA signals received from targets located at different depths. In reality, the diffraction effect is less dramatic, being altered by focusing abilities of the probe.

Our *in vivo* result supports the notion that OA imaging could complement the TRUS in identification of cancerous masses in the prostate as well as other blood-containing lesions. To supply a sufficient amount of nutrients and oxygen to their rapidly proliferating cells, tumors must incorporate

new blood vessels to sustain growth beyond 2 to 3 mm. OA imaging therefore shows considerable potential for identification of early stage malignancies with elevated microvessel density[17] but with weak mechanical contrast that would likely be missed by TRUS. As seen in Fig. 4(d), though anatomical features such as the urethra and bloody lesion can be identified in the OA image, they appear distorted due to acoustic diffraction. The urethra appears undistorted in the US image and the path of a needle insertion is identifiable, while the blood-filled lesion cannot be distinguished along the needle insertion path.

It should be noted that the induced lesion in our *in vivo* experiments likely has higher blood content than malignant tissue. It has been reported, though, that prostate carcinomas have significantly higher microvessel densities than surrounding tissues or benign lesions.[34] We anticipate that malignant tissue could still be resolved with OA imaging, and this is supported by our modeled image, in which the lesion's absorption coefficient was less than 10% of reported[35] $\mu_a$ of blood (9.1 cm$^{-1}$). In practice, although the absorption contrast of tumors would likely be diminished compared to the induced lesion in our *in vivo* experiments, cancerous lesions could still be identified, particularly with suitable filtering and dynamic range adjustments. Additionally, it must also be noted that our lesion model for prostate malignancy is better suited for OA imaging than for US imaging. During our experimental design, we found that, because the acoustic properties of endogenous tissue cannot be altered easily, mimicking a lesion *in vivo* suitable for both imaging modalities would prove challenging. Our presented results with the current lesion model demonstrate the benefits of combining both imaging modalities and encourage future experiments with surgically excised cancerous prostate tissue.

The presented OA images in Figs. 2–4 show objects elongated in the transverse direction. This phenomenon is well known in OA tomography, and is related to the limited aperture of the used US probe.[36] One way to improve transverse resolution of OA images of the prostate is to use *a priori* information on the characteristic structural features (prostate boundaries, urethra, etc.) in the reconstruction algorithm.[37] These structural features can be independently obtained using the same probe in the TRUS mode, and spatially correlated with the corresponding OA image. Such a straightforward approach justifies our current efforts in developing the dual modality OA-US system for imaging the human prostate.

## 5 Conclusion

In the course of the reported work, we found supportive evidence that OA imaging has potential as a technique for *in vivo* visualization of optical absorption within prostate tissue. Our *in vivo* experiments demonstrated the capability of the OA imaging system to visualize a prostate lesion with a high volumetric fraction of blood that was not detected by TRUS. It is, therefore, likely that the OA imaging system can provide enhanced detection sensitivity for early stage aggressively growing malignancies in the prostate, although several challenges must first be addressed. We evaluated the benefits of both forward and backward illumination. Though it is more invasive, forward-mode illumination through the urethra can provide a more uniform sensitivity through the depth of prostate

gland due to the fact that factors such as acoustic diffraction and light attenuation affect the image in opposite directions.

We are currently developing a hybrid system that acquires both OA and US images in real time with a single TRUS probe for prostate diagnosis. Additionally, we are refining our image reconstruction algorithms to allow for improved lateral resolution of OA images. In future studies, the OA and US images will be coregistered to yield images with detailed structural information that emphasize areas with a high probability of malignancies.

## Acknowledgments

## References

1. *Cancer Facts & Figures 2009*, American Cancer Society, Atlanta (2009).
2. A. Jemal, R. Siegel, E. Ward, Y. Hao, J. Xu, and M. J. Thun, "Cancer statistics, 2009," *Ca-Cancer J. Clin.* **59**, 225–249 (2009).
3. S. Bracarda, O. d. Cobelli, C. Greco, T. Prayer-Galetti, R. Valdagni, G. Gatta, F. d. Braud, and G. Bartsch, "Cancer of the prostate," *Crit. Rev. Oncol. Hematol.* **56**, 379–396 (2005).
4. M. H. Wink, J. J. M. M. C. d. l. Rosette, C. A. Grimbergen, and H. Wijkstra, "Transrectal contrast enhanced ultrasound for diagnosis of prostate cancer," *World J. Urol.* **25**, 367–373 (2007).
5. R. G. Aarnink, H. P. Beerlage, J. J. M. C. H. D. L. Rosette, F. M. J. Debruyne, and H. Wijkstra, "Transrectal ultrasound of the prostate: innovations and future applications," *J. Urol.* **159**, 1568–1579 (1998).
6. T. Steuber, P. Helo, and H. Lilja, "Circulating biomarkers for prostate cancer," *World J. Urol.* **25**, 111–119 (2007).
7. E. Kuligowska, M. A. Barish, H. M. Fenlon, and M. Blake, "Predictors of prostate carcinoma: accuracy of gray-scale and color Doppler US and serum markers," *Radiology* **220**, 757–764 (2001).
8. K. E. E. Din and J. J. M. C. H. D. L. Rosette, "Transrectal ultrasonography of the prostate," *Br. J. Urol.* **78**, 2–9 (1996).
9. W. L. Smith, C. Lewis, G. Bauman, G. Rodrigues, D. D'Souza, R. Ash, D. Ho, V. Venkatesan, D. Downey, and A. Fenster, "Prostate volume contouring: a 3D analysis of segmentation using 3DTRUS, CT, and MR," *Int. J. Radiat. Oncol., Biol., Phys.* **67**, 1238–1247 (2007).
10. H. Hricak, P. L. Choyke, S. C. Eberhardt, S. A. Leibel, and P. T. Scardino, "Imaging prostate cancer: a multidisciplinary perspective," *Radiology* **243**, 28–53 (2007).
11. Z. Jiang, D. Piao, G. Xu, J. W. Ritchey, G. R. Holyoak, K. E. Bartels, C. F. Bunting, G. Slobodov, and J. S. Krasinki, "Trans-rectal ultrasound-coupled near-infrared optical tomography of the prostate part II: experimental demonstration," *Opt. Express* **16**, 17505–17520 (2008).
12. Z. Jiang, G. Reed Holyoak, K. E. Bartels, J. W. Ritchey, G. Xu, C. F. Bunting, G. Slobodov, J. S. Krasinki, and D. Piao, "*In vivo* trans-rectal ultrasound coupled trans-rectal near-infrared optical tomography of canine prostate bearing transmissible venereal tumor," in *Optical Tomography and Spectroscopy of Tissue VIII*, B. J. Tromberg, A. G. Yodh, M. Tamura, E. M. Sevick-Muraca, and R. R. Alfano, *Proc. SPIE* **7174**, 71741U (2009).
13. A. A. Oraevsky, S. L. Jacques, R. O. Esenaliev, and F. K. Tittel, "Time-resolved optoacoustic imaging in layered biological tissues," in *OSA Proc. on Advances in Optical Imaging and Photon Migration*, R. R. Alfano, Ed., Vol. **21**, pp. 161–165 (1994).
14. A. A. Oraevsky and A. A. Karabutov, "Optoacoustic tomography," in *Biomedical Photonics Handbook*, T. Vo-Dinh, Ed., pp. 34-31––34-34, CRC Press, Boca Raton, FL (2003).
15. V. G. Andreev, A. A. Karabutov, and A. A. Oraevsky, "Detection of ultrawide-band ultrasound pulses in optoacoustic tomography," *IEEE Trans. Ultrason. Ferroelectr. Freq. Control* **50**, 1383–1390 (2003).
16. R. O. Esenaliev, A. A. Karabutov, and A. A. Oraevsky, "Sensitivity of laser opto-acoustic imaging in detection of small deeply embedded tumors," *IEEE J. Sel. Top. Quantum Electron.* **5**, 981–988 (1999).
17. B. Nicholson, G. Shaefer, and D. Theodorescu, "Angiogenesis in prostate cancer: Biology and therapeutic opportunities," *Cancer Metastasis Rev.* **20**, 297–319 (2001).
18. M. Choy and S. Rafii, "Role of angiogenesis in the progression and treatment of prostate cancer," *Cancer Invest* **19**, 181–191 (2001).
19. M. Çetinkaya, S. Günçe, E. Ulusoy, F. Aksoy, Ö. Yildiz, Ö. Adsan, and C. Özden, "Relationship between prostate specific antigen density, microvessel density, and prostatic volume in benign prostatic hyperplasia and advanced prostatic carcinoma," *Int. Urol. Nephrol.* **30**, 581–585 (1998).
20. W. H. Nau, R. J. Roselli, and D. F. Milam, "Measurement of thermal effects on the optical properties of prostate tissue at wavelengths of 1,064 and 633 nm," *Lasers Surg. Med.* **24**, 38–47 (1999).
21. T. Svensson, S. Andersson-Engels, M. Einarsdóttír, and K. Svanberg, "In vivo optical characterization of human prostate tissue using near-infrared time-resolved spectroscopy," *J. Biomed. Opt.* **12**, 014022 (2007).
22. M. R. Arnfield, J. D. Chapman, J. Tulip, M. C. Fenning. and M. S. McPhee, "Optical properties of experimental prostate tumors in vivo," *Photochem. Photobiol.* **57**, 306–311 (1993).
23. T. D. Khokhlova, I. M. Pelivanov, V. V. Kozhushko, A. N. Zharinov, V. S. Solomatin, and A. A. Karabutov, "Optoacoustic imaging of absorbing objects in a turbid medium: ultimate sensitivity and application to breast cancer diagnostics," *Appl. Opt.* **46**, 262–272 (2007).
24. S. Manohar, A. Kharine, J. C. G. v. Hespen, W. Steenbergen, and T. G. v. Leeuwen, "Photoacoustic mammography laboratory prototype: imaging of breast tissue phantoms," *J. Biomed. Opt.* **9**, 1172–1181 (2004).
25. S. Manohar, A. Kharine, J. C. G. v. Hespen, W. Steenbergen, and T. G. v. Leeuwen, "The Twente photoacoustic mammoscope: system overview and performance," *Phys. Med. Biol.* **50**, 2543–2557 (2005).
26. S. A. Ermilov, A. Conjusteau, K. Mehta, R. Lacewell, P. M. Henrichs, and A. A. Oraevsky, "128-channel laser optoacoustic imaging system (LOIS-128) for breast cancer diagnostics," in *Photons Plus Ultrasound: Imaging and Sensing 2006: The 7th Conf. on Biomedical Thermoacoustics, Optoacoustics, and Acousto-optics*, A. A. Oraevsky, Ed., **6086**, 68–79 (2006).
27. S. A. Ermilov, M. P. Fronheiser, H.-P. F. Brecht, R. Su, A. Conjusteau, K. Mehta, P. Otto, and A. A. Oraevsky, "Development of laser optoacoustic and ultrasonic imaging system for breast cancer utilizing handheld array probes," in *Photons Plus Ultrasound, Photonics West*, A. A. Oraevsky and L. V. Wang, Eds., *Proc. SPIE* **7177**, 717703 (2009).
28. J. J. Niederhauser, M. Jaeger, R. Lemor, P. Weber, and M. Frenz, "Combined ultrasound and optoacoustic system for real-time high-contrast and vascular imaging *in vivo*," *IEEE Trans. Med. Imaging* **24**, 436–440 (2005).
29. S. A. Ermilov, T. Khamapirad, A. Conjusteau, M. H. Leonard, R. Lacewell, K. Mehta, T. Miller, and A. A. Oraevsky, "Laser optoacoustic imaging system for detection of breast cancer," *J. Biomed. Opt.* **14**, 024007 (2009).
30. A. A. Oraevsky, V. G. Andreev, A. A. Karabutov, and R. O. Esenaliev, "Two-dimensional optoacoustic tomography: transducer array and image reconstruction algorithm," in *Laser-Tissue Interaction X: Photochemical, Photothermal, and Photomechanical*, S. L. Jacques, G. J. Mueller, A. Roggan, and D. J. Sliney, Eds., *Proc. SPIE* **3601**, 256–267 (1999).
31. M. A. Yaseen, H. P.-F. Brecht, S. A. Ermilov, R. Gharieb, A. Conjusteau, and A. A. Oraevsky, "Hybrid optoacoustic and ultrasonic imaging system for detection of prostate malignancies," in *Photons Plus Ultrasound: Imaging and Sensing*, A. A. Oraevsky and L. V. Wang, Eds., *Proc. SPIE* **6856**, 68560T (2008).
32. L. Wang, S. L. Jaques, and L. Zheng, "MCML—Monte Carlo modeling of light transport in multi-layered tissues," *Comput. Methods Programs Biomed.* **47**, 131–146 (1995).
33. A. A. Oraevsky, S. A. Ermilov, K. Mehta, T. Miller, B. A. Bell, E. Orihuela, and M. Motamedi, "*In vivo* testing of laser optoacoustic system for image-guided biopsy of prostate," in *Photons Plus Ultrasound, Photonics West*, A. A. Oraevsky and L. V. Wang, Eds., *Proc. SPIE* **6086**, 80–90 (2006).
34. M. K. Brawer, R. E. Deering, M. Brown, S. D. Preston, and S. A. Bigler, "Predictors of pathologic stage in prostatic carcinoma: the

role of neovascularity," *Cancer* **73**, 678–687 (1994).

35. A. Roggan, M. Friebel, K. Doerschel, A. Hahn, and G. J. Mueller, "Optical properties of circulating human blood in the wavelength range 400–2500 nm.," *J. Biomed. Opt.* **4**, 36–46 (1999).

36. M. Xu and L. V. Wang, "Analytic explanation of spatial resolution related to bandwidth and detector aperture size in thermoacoustic or photoacoustic reconstruction," *Phys. Rev. E Stat. Phys. Plas. Fluids*

*Rel. Interdiscipl. Top.* **67**, 056605 (2003).

37. J. Gamelin, A. Aguirre, A. Maurudis, L. V. Wang, and Q. Zhu, "Improvements in time resolution of tomographic photoacoustic imaging using a priori information for multiplexed systems," in *Photons Plus Ultrasound: Imaging and Sensing*, A. A. Oraevsky and L. V. Wang, Eds., *Proc. SPIE* **7177**, 71771C (2009).